Coupled Dynamics and Sediment Transport in a Human-modified Estuarine Network

Final Report to the Hudson River Foundation
Grant #GF/01/17

W. Bryce Corlett
Woods Hole Oceanographic Institution
266 Woods Hole Rd.
Woods Hole, MA 02543

and

W. Rockwell Geyer
Woods Hole Oceanographic Institution
266 Woods Hole Rd.
Woods Hole, MA 02543

December 21, 2018

1 Research Summary

This report describes the results of Hudson River Foundation Mark B. Bain graduate fellowship #GF/01/17, which was awarded to study the effects of bathymetric change on the dynamics and sediment transport of the Newark Bay estuarine network. The shape and depth of Newark Bay has been substantially modified over the past 150 years; the western shoreline has been reclaimed and reconfigured to form Port Newark and Port Elizabeth, and the channel has been deepened by roughly 300% from 4 to 17 m. Similar modifications in estuaries in western Europe have amplified local concentrations of suspended sediment by up to an order of magnitude, producing an unsustainable feedback loop between channel deepening and the import of sediment. These effects have not been observed in Newark Bay, prompting our investigation to determine why this network has reacted differently to human-driven modifications. The original objectives of this study were the following:

1. identify and quantify the key processes responsible for sediment trapping in Newark Bay, with particular attention to the relative roles of local and nonlocal (i.e., from the Hudson River and New York Harbor) forcing;

2. characterize the mechanisms of salt front formation and propagation as well as the influence of fronts on sediment transport and trapping; and

3. assess the effects of human-induced channel deepening on estuarine dynamics and sediment transport.

To address these objectives, five moorings were deployed within the estuarine network and surrounding waterways from May 17 through July 7, 2016. Each mooring measured temperature, salinity, and optical backscatter at 0.5 m above the bed and 1 m beneath the water's surface. Each mooring also measured vertical profiles of horizontal velocities and acoustic backscatter. Two shipboard hydrographic surveys during the mooring deployment revealed the formation and advection of four salt fronts within the sub-estuary. A comparison of shipboard data with the mooring-based salinity records demonstrated that these fronts are consistent features, and that frontal advection substantially contributes to both tidal and subtidal salinity variability within the estuarine network. Due to the importance of fronts on the dynamics and kinematics of the estuarine network, and a lack of suitable calibrations of backscatter to suspended sediment concentrations, the initial study objectives were modified to the following:

1. characterize the mechanisms of salt front formation and propagation;

2. quantify the contribution of tidal salt front propagation to the tidal-residual estuarine circulation; and

3. assess the effects of the channel geometry on the along-channel structure of the estuarine circulation.

The first two objectives are addressed with moored and shipboard hydrographic observations, and the third objective will be addressed through a combination of hydrographic observations and the results of a numerical model of the Newark Bay estuarine network. Details regarding the observations are described in §4. Preliminary results addressing objectives (1) and (2) were presented at the 2017 Coastal and Estuarine Research Foundation Meeting, as well as the 2018 Physics of Estuaries and Coastal Seas Meeting. In addition, a manuscript characterizing the formation mechanisms of each front has been submitted for publication in *Estuaries and Coasts*. In the coming year, we expect to submit two more manuscripts for peer-reviewed publication which will address objectives (2) and (3). All results form the basis of Corlett's ongoing doctoral thesis, which will be complete in the summer of 2019.

2 Background

Partially-mixed estuaries are often portrayed as having near-uniform along-channel salinity and stratification gradients (Hansen and Rattray Jr. 1965; MacCready and Geyer 2010). However, observations frequently reveal significant variability in the strength of these gradients, especially in fjords. In Puget Sound, for example, horizontal gradients in salinity and stratification are larger over shallow sills than along deep basins (Ebbesmeyer and Barnes 1980). At bathymetric transitions, horizontal salinity gradients are concentrated in fronts (Lavelle et al. 1991); during flood tides, the fronts are advected into basins as gravity currents, driving the tidal-residual renewal of dense basin water (Geyer and Cannon 1982). These fronts also divide the fjord into a series of distinct segments, creating a system of mixing zones and advective reaches (Cokelet and Stewart 1985). The effects of fronts within fjords may be relevant to partially-mixed and well-mixed estuarine regimes as well, as fronts form in all types of estuaries (Largier 1993; Geyer and Ralston 2015).

Along-channel estuarine fronts are generated by a variety of mechanisms, which are manifest in the tendency equation of the along-channel salinity gradient, derived from the along-estuary derivative of the salt conservation equation:

$$\underbrace{\frac{\partial}{\partial t}\frac{\partial s}{\partial x}}_{1} + \underbrace{u \cdot \nabla \frac{\partial s}{\partial x}}_{2} = \underbrace{-\frac{\partial u}{\partial x}\frac{\partial s}{\partial x}}_{3} \underbrace{-\frac{\partial v}{\partial x}\frac{\partial s}{\partial y}}_{4} \underbrace{-\frac{\partial w}{\partial x}\frac{\partial s}{\partial z}}_{5} \underbrace{-\frac{\partial}{\partial x}\frac{\partial(\overline{s'w'})}{\partial z}}_{6} \tag{1}$$

This equation describes the tendency (term 1) and advection (term 2) of the local salinity gradient, as well as the generation of along-channel fronts through the convergence of the along-channel salinity gradient (term 3), the twisting of a cross-channel gradient (term 4), the shearing of stratification (term 5), and the sharpening of the along-channel salinity gradient by a mixing gradient (term 6). Although all of these mechanisms may generate fronts, frontogenesis by along-channel convergence is most commonly discussed (Simpson and Nunes 1981; Largier 1992; MacDonald and Geyer 2005; Ralston et al. 2010).

During formation, lift-off fronts are essentially arrested gravity currents (Benjamin 1968), in which the baroclinic propagation speed of the front matches the speed of the oncoming flow. Consequently, the internal hydraulic state of the flow is often critical at locations of frontogenesis (Armi and Farmer 1986). After the change of tide, these fronts tend to propagate landward as gravity currents; Geyer and Farmer (1989), for example, described the landward propagation of a lift-off front as a salt wedge during flood tide at the mouth of the Fraser River. In some cases, these propagating fronts induce the formation of new bottom fronts during the following ebb tide by initiating along-channel convergences at more landward locations (Simpson and Linden 1989).

Fronts also form at bathymetric transitions through non-buoyant processes. At channel confluences, for example, laterally-convergent streams produce fronts (Best 1987; Rhoads and Sukhodolov 2001). When the confluence is asymmetric, i.e., one of the flows is stronger than the other, the resulting lateral shear may rotate the front into the along-channel direction (De Serres et al. 1999; Riley et al. 2014). These fronts may also exhibit cross-front buoyancy gradients, which are produced by either contrasting water properties (Farmer et al. 1995) or tidal phase-shifts between channels (Warner et al. 2002; Giddings et al. 2012).

Confluence fronts and lift-off fronts both form at channel junctions, located either within an estuary or between an estuary and the receiving waters (e.g., lift-off fronts). These junctions provide either the geometry or phase-shifts that are conducive to frontogenesis. Phase-shifts at junctions may also modify the process of frontogenesis by altering the horizontal salinity gradient (Pritchard and Bunce 1959; Alebregtse et al. 2013) and the along-channel velocity gradient (Warner et al. 2003). Warner et al. (2002), for example, observed that phase-shifts between channels may generate either convergent or divergent along-channel salinity gradients at a junction depending on the phase of the tide. A phase-shift at a junction between a channel and side channel may enhance the lateral salinity gradient, generating a lateral bottom front (van Maren et al.

2009). These bottom fronts propagate into side channels as part of a tidal lock exchange process produced by the channel—side channel phase-shift (Allen and Price 1959; Hayward et al. 1982). The lock exchange may also influence the along-channel salinity gradient by alternately exporting freshwater into the main channel at the surface and saline water into the main channel at the bed.

Tidal oscillations of the along-channel salinity gradient generate residual salt fluxes when the tidal phases of velocity and salinity are out of quadrature (Larsen 1977). In the Puget Sound, for example, lift-off fronts that propagate as gravity currents generate residual fluxes by advecting salt water landward during flood tide and not returning seaward during ebb tide (Geyer and Cannon 1982). Dronkers and van de Kreeke (1986) described the contribution of advected features to the local estuarine circulation as the "nonlocal" component of the salt flux, which they inferred from hydrographic observations of the Volkerak estuary to be largest in a region characterized by salt fronts. As these contributions are formulated as dispersive rather than advective processes in Eulerian coordinates, Wang et al. (2015) found that the terms are more accurately described through the Total Exchange Flow (TEF) framework (MacCready 2011). This framework enables accurate estimates of tidal oscillatory salt fluxes as part of the total residual salt flux, and enables the dissection of physical mechanisms that contribute to these fluxes. We hypothesize that the TEF framework also enables the quantification of the effects of frontal advection on the tidal oscillatory salt flux. The framework may additionally provide insight into the spatial structure of the exchange flow in regions of partially- or well-mixed estuarine systems characterized by abrupt geometric transitions.

In this report, we examine how junctions affect the formation of salinity fronts, and how these fronts contribute to exchange flow of a partially-mixed estuarine network. The structure of the paper is as follows: section 3 describes the site, Newark Bay; section 4 reports our methods; section 5 presents results regarding the observed mechanisms of frontogenesis and the influence of fronts on the exchange flow; and section 6 reports the conclusions of this study. The influence of frontal propagation on the along-channel structure of the exchange flow will be discussed in future publications as the analysis is ongoing.

3 Site description

Newark Bay, New Jersey is a sub-estuary of the Hudson River—New York Harbor estuary (Fig. 1), and is connected to the Harbor through Kill van Kull, and to Raritan Bay through Arthur Kill. New York Harbor and each of the connecting straits are roughly 20 m deep. At the junction between the Harbor and Kill van Kull, the width of the channel abruptly decreases by one-third. The channel is further punctuated by a series of abrupt bathymetric transitions within the sub-estuary, which are due to the natural geometry of the system as well as human-induced channel modifications. These modifications include two side channels associated with Port Newark and Port Elizabeth, and an abrupt shoaling of the channel from 17 m to 13 m in the middle of Newark Bay. At the northern end of Newark Bay, the channel splits into the Passaic and Hackensack Rivers; the channel shoals from 13 m to 6 m at the mouth of the Passaic.

Tides within the sub-estuary are largely semidiurnal, with a mean range of 1.5 m (Mathew and Winterwerp 2017). Tidal velocity and water level are 90 degrees out of phase throughout the Newark Bay estuarine network (Chant et al. 2011). Tidal velocity and water level are 45 degrees out of phase in the adjacent Hudson River (Nepf and Geyer 1996); consequently, tidal velocities within the Harbor lag velocities within the sub-estuary by 45 degrees, or roughly 90 minutes. Newark Bay is a partially-mixed estuary, with modest to moderate stratification and a robust two-layer estuarine exchange flow (Suszkowski 1978; Chant et al. 2018). Most freshwater (85%) enters Newark Bay from the Passaic River; however, the Passaic River tidal prism is roughly one-quarter of the size of the Hackensack River tidal prism (Shrestha et al. 2014). Most seawater enters the sub-estuary through Kill van Kull, in response to a net clockwise circulation around Staten Island (Suszkowski 1978; Blumberg et al. 1999). This circulation pattern is produced by

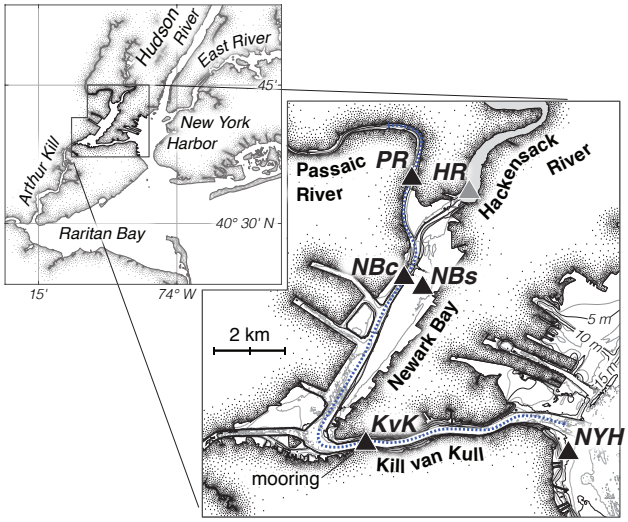

Fig. 1 The Newark Bay estuarine network, showing locations of moorings and the along-channel hydrographic sections. Moorings in 2008 are shown in gray, and moorings in 2016 are shown in black. The inset depicts the surrounding waterways.

a mean sea level gradient between the mouth of Kill van Kull in New York Harbor and the mouth of Arthur Kill in Raritan Bay (Kaluarachchi et al. 2003).

4 Methods

Shipboard and moored observations of the Newark Bay estuarine network and New York Harbor were conducted in the spring and early summer of 2016. Five moorings were deployed within the sub-estuary network from March 17 through July 7, each within a region of unique lateral channel geometry. From south to north, these moorings are labelled New York Harbor (NYH), Kill van Kull (KvK), Newark Bay channel (NBc), Newark Bay shoal (NBs), and Passaic River (PR; Fig. 1). All moorings were equipped with near-bed and near-surface conductivity-temperature sensors, which measured temperature and salinity once per minute at two depths: 0.5 m above the bed and 1 m below the water surface. Each mooring was also equipped with an upward-facing acoustic Doppler current profiler (ADCP), which measured vertical profiles of horizontal velocities every ten minutes in 50 cm depth-bins from 0.5 m above the bed through 1 m below the water surface. Velocity measurements at mooring PR were not recovered due to internal corrosion of the ADCP by seawater; the housing of the ADCP was breached by a propeller while deployed. In addition, some data loss occurred at all moorings due to biofouling. Consequently, the period of full moored data coverage ceases on May 30. All mooring-based data were interpolated onto a ten-minute sampling interval for processing and analysis.

Characteristics of the Passaic and Hackensack rivers that are presented in §5.3 were determined from mooring-based measurements of salinity and horizontal velocity collected from September 17 through November 30, 2008 as part of HRF Grant #008/07A (Sommerfield and Chant 2010). Freshwater discharge and tidal velocities during this period are statistically similar to conditions during the 2016 mooring deployment, enabling a direct comparison of mean characteristics along the axis of the sub-estuary.

To capture the along- and across-channel variability of estuarine characteristics, shipboard measurements of velocity and salinity were made over semidiurnal tidal periods using downward-facing 1200 kHz ADCPs and continuously-profiling 12 Hz conductivity-temperature-depth (CTD) sensors. ADCPs measured horizontal velocities in 0.25 m depth-bins every second, or roughly every 2.5 m, and CTDs measured salinity and temperature with a vertical resolution of 0.1 m every 70 m. For the following analyses, shipboard data were subsampled onto the vertical resolution of ADCP measurements and the horizontal resolution of CTD measurements. Shipboard surveys took place during two periods of the 2016 mooring deployment. The first (May 11–14) occurred during

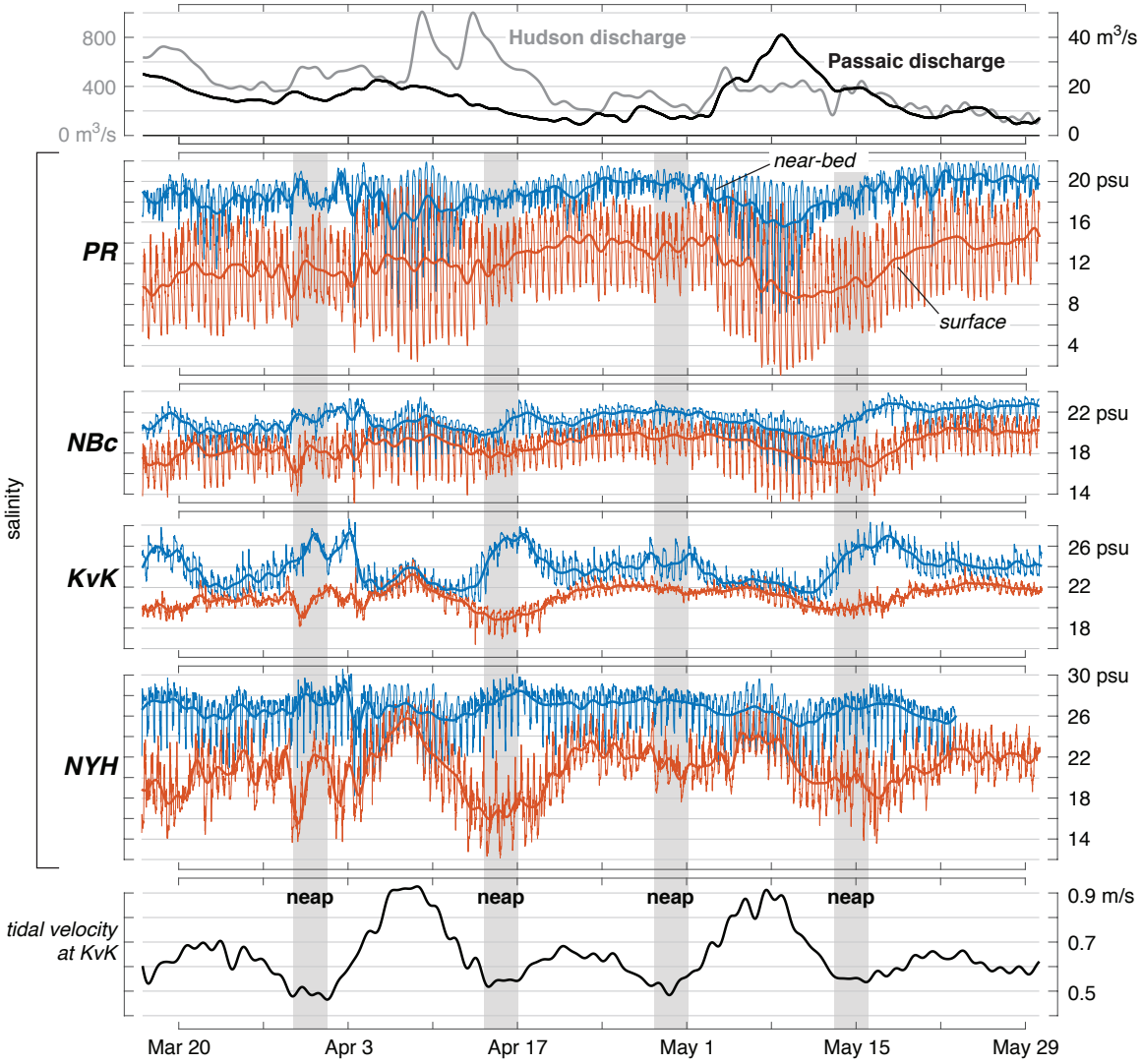

Fig. 2 Time series of environmental conditions and salinity over the period of full moored data coverage. 33-hour filtered salinity measurements are superimposed over 10-minute data to show subtidal variability.

perigean spring tides and relatively high freshwater discharge conditions (Fig 2, top panel). The second period (June 30–July 1) coincided with low discharge conditions and apogean spring tides.

5 Results and interpretation

5.1 Overall structure of the estuarine network

During the 2016 deployment, discharge conditions within the Passaic River and Hackensack Rivers were below historically average conditions; the combined mean discharge was 15 m^3/s (Fig. 2 — the 6^{th} percentile of the seasonal climatology during the deployment period (USGS gages 01389500 and 01378500, 1920–2015). Freshwater discharge in the Hudson River was also below average relative to the seasonal climatology (at the 9^{th} percentile; USGS gage 01358000, 1946–2015). The tidal range within the Newark Bay estuarine network was larger than average;

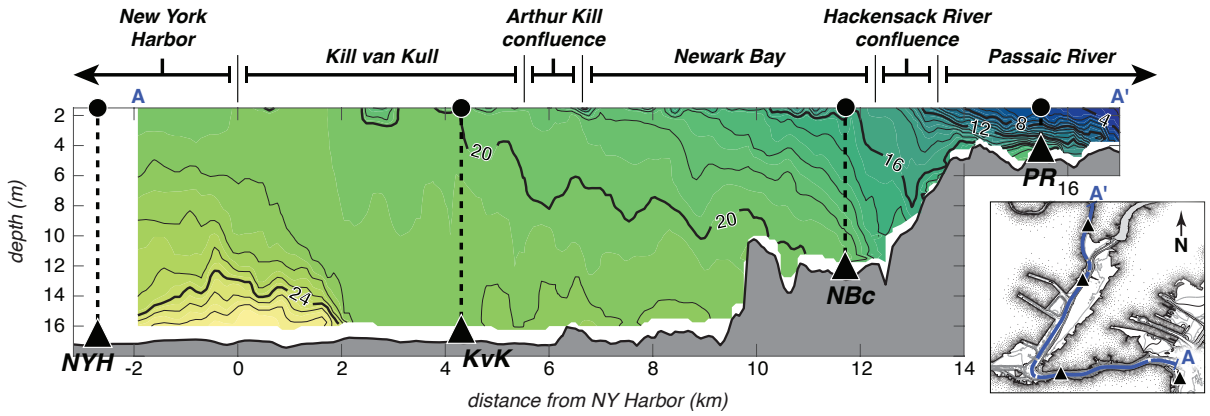

Fig. 3 Mooring locations relative to the end-of-ebb along-channel salinity structure of the sub-estuary during spring tides and high discharge. Isohalines are indicated with both black contour lines and color shading.

spring tides aligned with lunar perigee during the deployment, creating two larger-than-average perigean spring tides and three apogean spring tides (Fig. 2, bottom panel). From neap tides to perigean spring tides, the tidal amplitude ranged from roughly 0.5–1.0 m, and depth-averaged tidal velocities ranged from 0.5–0.9 m/s.

Measurements of salinity at each mooring reveal fluctuations on time scales of the semidiurnal tide, the fortnightly spring/neap cycle, and freshwater discharge events. Subtidal salinity fluctuations in New York Harbor are primarily influenced by the spring/neap cycle, which significantly decreases the surface salinity measured at mooring NYH during neap tides. Within the Newark Bay estuarine network, spring/neap fluctuations are most evident in near-bed salinity, which increases by up to 5 psu at the mouth of the sub-estuary during neap tides. This response rapidly weakens toward the head of the network. Within the Passaic River, subtidal variability is mostly influenced by fluctuations in river discharge. Tidal fluctuations in salinity and stratification are most visible at moorings PR and NYH; however, similar rapid variations in salinity on tidal time scales are also observed at the other channel moorings. This suggests that the dominant length of along-channel salinity variability is less than a tidal excursion.

The spatial heterogeneity of salinity and stratification is confirmed by an along-channel hydrographic section obtained at the end of ebb tide (Fig 3). Although the section presents a snapshot of tidal conditions, its depiction of the estuarine network is consistent with the mean characteristics of the moored time series. Stratification is largest at the landward and seaward boundaries of the network. Conditions within Newark Bay are partially-mixed, and Kill van Kull is largely well-mixed. Between regions of different stratification, the along-channel salinity gradient is concentrated in fronts. A bottom front separates the Harbor from Kill van Kull, and a surface front separates the Passaic River from the Hackensack River confluence. Salinity and stratification gradients are more gradual between Kill van Kull and Newark Bay; however, a weak bottom front is observed near 12 km, and a weak surface front is observed near 10 km.

5.2 Frontogenesis at estuarine junctions

The salinity measured at each mooring rapidly increases during flood tide, consistent with the passage of fronts. Fronts that are advected landward during flood tide rapidly increase the salinity measured at a stationary mooring, as the sharp horizontal salinity gradient is translated into a rapid temporal change in salinity. The tidal cycles that contain these rapid changes in salinity are shown in grey in Figure 4; repeated hydrographic sections (discussed below) confirm that these tidal fluctuations are indeed generated by advected salinity fronts. This process of identifying advected fronts within the moored salinity records reveals that bottom fronts pass moorings KvK

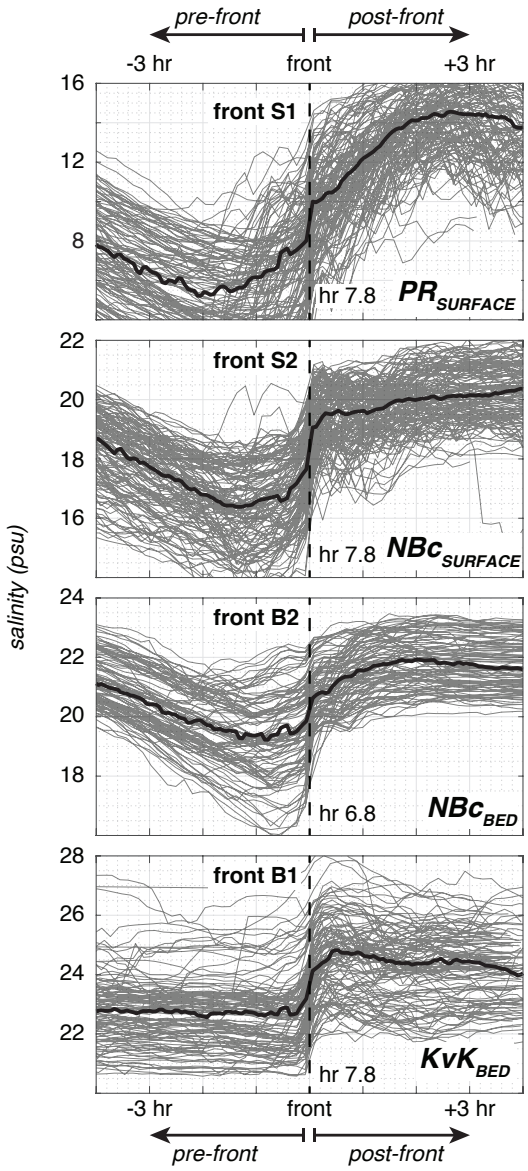

Fig. 4 Temporal increases in salinity attributed to the landward advection of fronts at each mooring; advected fronts are associated with temporal increases in salinity at least two standard deviations larger than the mean temporal salinity gradient. Time series are aligned such that all fronts occur at the mean tidal hour of frontal advection, and average tidal salinity variability at each mooring after co-locating frontal measurements is shown in black. Tidal hours are given in reference to the depth-averaged velocity at each mooring; hour 0 occurs at the start of ebb tide, and hour 6 occurs at the start of flood tide. Note that the salinity scale at mooring *PR* is twice as large as the scales at moorings *NBc* and *KvK*.

and NBc in over 70% of tidal cycles, and surface fronts pass moorings PR and NBc in over 90% of tidal cycles.

The consistent observations of frontal advection throughout the three-month record permit the characterization of the fronts at each mooring. The recurrent bottom fronts at moorings KvK and NBc (labelled B1 and B2) both increase near-bed salinity by an average of 2 psu in early flood tide. Subtidal salinity variability at mooring KvK is primarily restricted to the mean flood tide salinity, which decreases by roughly 3 psu from neap tides to perigean spring tides. At mooring NBc, on the other hand, fluctuations in the spring/neap cycle significantly influence the salinity difference across front B2; the salinity difference increases by an average of 1.7 psu from neap tides to perigean spring tides. The relationship between the strength of the front and the spring/neap cycle suggests that the process of frontogenesis for front B2 is influenced by the tidal salinity range. The recurring surface front at mooring NBc (labelled S1) increases the surface salinity by an average of 3 psu in early flood tide. The salinity difference across front S1 significantly increases by an average of 1.7 psu from neap tides to perigean springs, similar to front B2, which suggests that fronts B2 and S1 may be generated by similar tidal processes. The salinity

difference across the recurring surface front at mooring PR (labelled S2), on the other hand, is primarily influenced by fluctuations in river flow. Front S2 increases the near-surface salinity by an average of 4 psu during low discharge, and an average of 8 psu during peak discharge. These fluctuations in salinity difference produce the vertical spread of salinity measurements shown in Figure 4.

Repeated hydrographic surveys in each region of the sub-estuary provide insight into the formation and evolution of these fronts. All fronts observed at the moorings form at junctions during ebb tide. The fronts are generated by flow through junctions, and most of the fronts are modified by tidal phase-shifts. While there are similarities among the frontal locations, each front demonstrates a different mechanism through which junctions influence frontogenesis and frontal evolution.

Front B1. The formation and tidal evolution of front B1 within Kill van Kull is shown in two-hour increments in Figure 5. At the start of ebb tide (hour 0.7), the near-bed salinity gradient in Kill van Kull is nearly uniform, and ebb velocities accelerate seaward at the 500-meter channel expansion at the mouth of Kill van Kull. Near-bed velocities reverse direction roughly one kilometer seaward of the mouth due to the tidal velocity phase-shift between New York Harbor and the Newark Bay estuarine network; flood tide within the Harbor ends 90 minutes after the start of ebb tide in Kill van Kull. As ebb tide progresses (hour 2.5), the along-channel salinity gradient is concentrated into front B1 by convergent near-bed velocities at 0 km (Eq. 1, term 1). Flow within Kill van Kull during ebb tide is supercritical, and the lift-off of the isohaline associated with front B1 is consistent with the response of seaward supercritical flow to a seaward channel expansion (MacDonald and Geyer 2005; Armi and Farmer 1986). This suggests that front B1 is a lift-off front, generated by the response of ebb flow to the abrupt channel expansion at the mouth of Kill van Kull. This process is enhanced by the tidal velocity phase-shift between the Harbor and the Newark Bay estuarine network, which both reverses flow on the seaward side of the channel expansion (demonstrated in hour 0.7) and increases the along-channel salinity gradient by increasing the salinity on the seaward side of the front. Consequently, front B1 forms in early ebb tide whereas most lift-off fronts form during late ebb (Geyer and Ralston 2015). The front is also modified by the tidal velocity phase-shift during early flood (hours 6.2–8.3), as flood tide in Kill van Kull precedes the beginning of flood tide in New York Harbor by 90 minutes. The persistent ebb tide in the Harbor advects fresh surface water into the Kill van Kull from the adjacent Hudson River, reversing the along-channel salinity gradient at the mouth. This detaches the propagating gravity current behind front B1 from the Harbor, making front B1 visibly different from lift-off fronts observed at the mouths of salt-wedge estuaries (Geyer and Farmer 1989; Ralston et al. 2010), which tend to have along-channel salinity gradients that monotonically increase toward the sea.

Front B2. The formation and tidal evolution of bottom front B2 is shown in Figure 6 in roughly ninety-minute intervals. The salinity field within Newark Bay is nearly uniform in early ebb tide (hour 1.5), and near-bed velocities are weakly divergent. By maximum ebb tide (hour 3.0), near-bed velocities at 10.5 km are convergent, drawing the along-channel salinity gradient closer together and generating bottom front B2 (Eq. 1, term 1). The front forms at a seaward channel expansion at the mouth of the Port Newark side channel. As flow throughout the region is supercritical during ebb tide, we hypothesize that the front is generated by the lift-off response of ebb flow to the side channel. However, the front remains in the same location into late ebb despite persistent supercritical conditions (hour 4.3). Repeated lateral hydrographic sections at the side channel junction under similar environmental conditions reveal that the front remains stationary due to barotropic and baroclinic tidal velocity phase-shifts between the main channel and side channel. These lateral sections are shown in Figure 7 in roughly ninety-minute intervals from the end of flood tide through early flood tide (note the lower salinity—the 20 psu isohaline corresponds to the 24 psu isohaline in Fig. 6). The near-bed salinity of the main channel is greater than the side channel from the end of flood through early ebb tide (hours 11.8–1.3); the combination of this baroclinic pressure gradient with a lateral barotropic pressure gradient generates a lateral circulation in which salt water is advected into the side channel at the bed. As ebb tide progresses (hours 2.7–4.2), the near-bed salinity in the main channel decreases due to the seaward advection

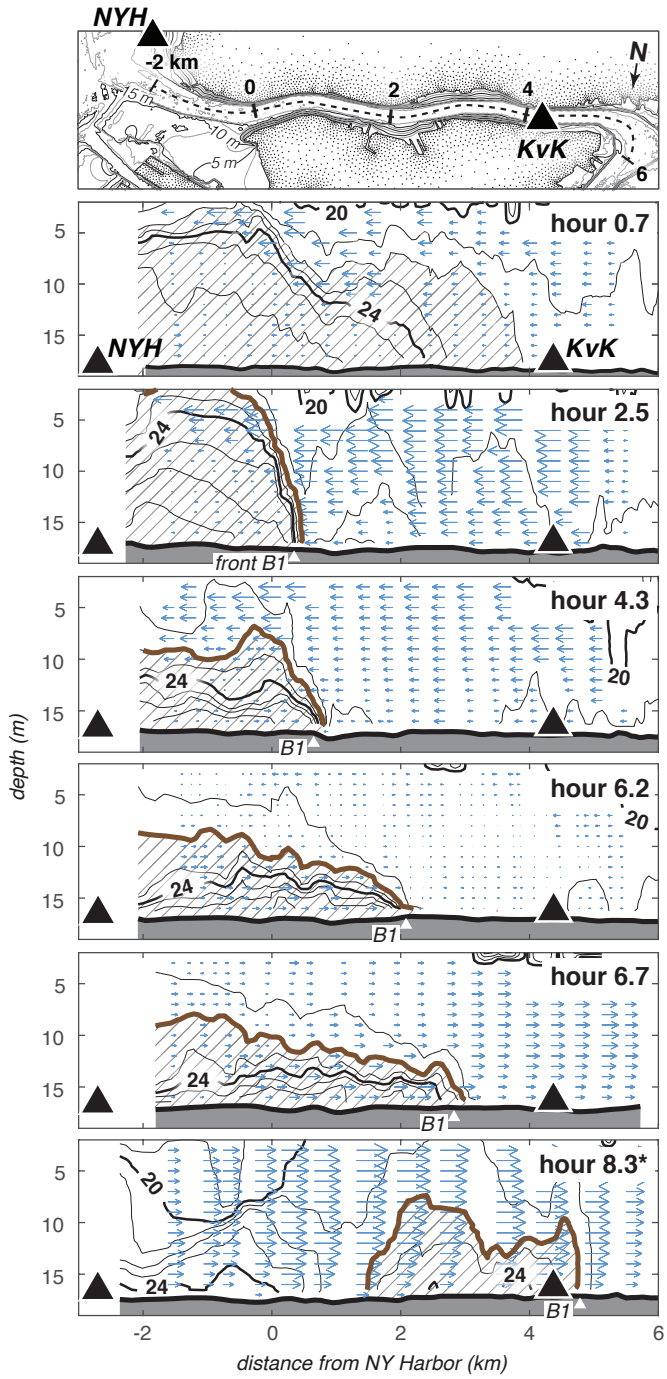

Fig. 5 Repeated along-channel salinity sections in Kill van Kull from the start of ebb tide (hour 0.7) through maximum flood (hour 8.3). Along-channel velocities are shown with arrows, and shading indicates salinities greater than 22 psu. *Conditions at maximum flood were observed at the end of the previous tidal cycle.

of fresh water from the Passaic and Hackensack rivers. By late ebb (hour 4.2), the low salinity of the main channel reverses the baroclinic circulation of the side channel. Consequently, salt water that was trapped in the side channel from the previous flood tide is expelled into the main channel on the seaward side of front B2; this is shown in Figure 6 as the bolus of 24 psu water at 10.5 km in late ebb (hours 4.3 and 6.2). The steady expulsion of salt water from the side channel during late ebb allows the front to persist as a boundary between fresh water from upstream and salt water from the side channel.

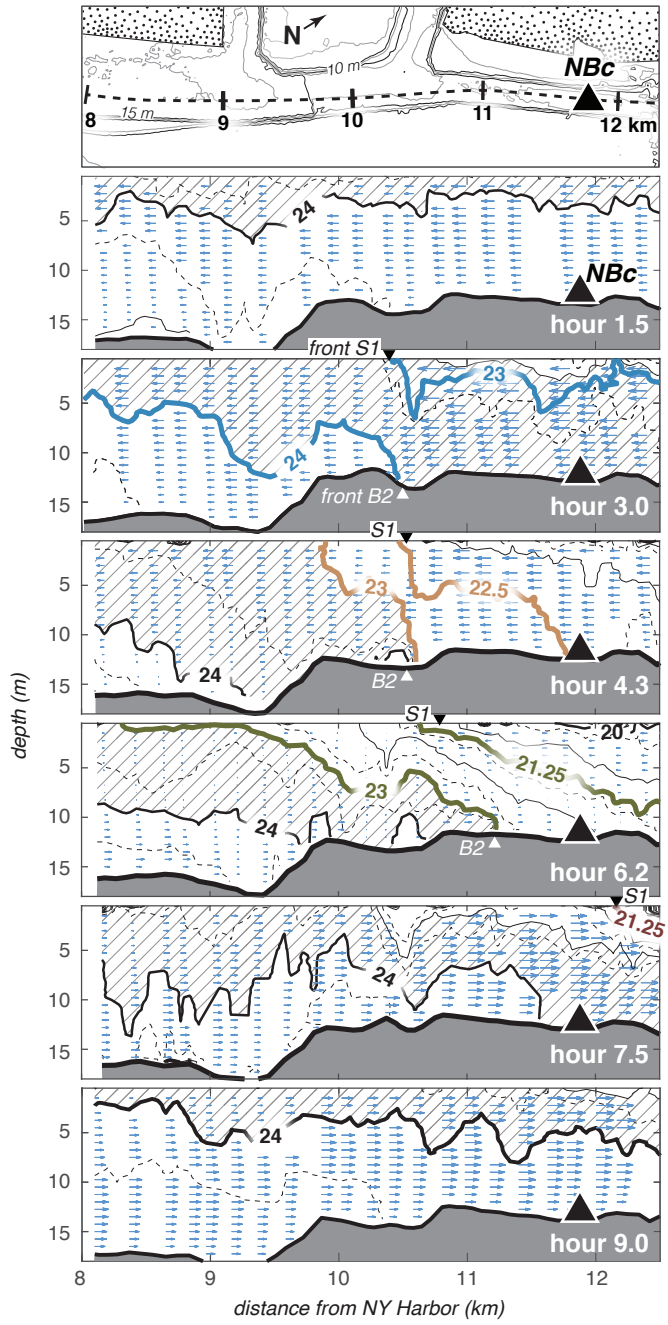

Fig. 6 Along-channel salinity sections in Newark Bay from early ebb tide (hour 1.5) through maximum flood (hour 9.0). Arrows indicate along-channel velocities, and shading corresponds to salinities between 23 and 24 psu. Isohalines associated with fronts B2 and S1 over time are highlighted with colors that correspond to the changes over time depicted in Figures 8 and 10.

Front S1. A surface front also forms during ebb tide at the mouth of the side channel (Fig. 6). In early ebb (hour 1.5), the surface velocities and salinity gradient throughout Newark Bay are nearly uniform. By maximum ebb (hour 3.0), surface velocities roughly double on the landward side of the side channel at 10.5 km, whereas those on the seaward side remain nearly constant. This convergence concentrates the along-channel salinity gradient into front S1 (Eq. 1, term 1), which persists at the mouth of the side channel through the end of ebb tide (hour 6.2) despite the steady seaward advection of salt water. Repeated lateral hydrographic sections during similar environmental conditions suggest that the along-channel convergence that forms front S1 is generated by the interaction of the main channel with the side channel; these sections are shown in Figure 7 from late flood tide to early flood tide. At the end of flood tide (hour 11.8; Fig. 7), the surface salinity within the side channel is less than the salinity in the main channel. The resulting

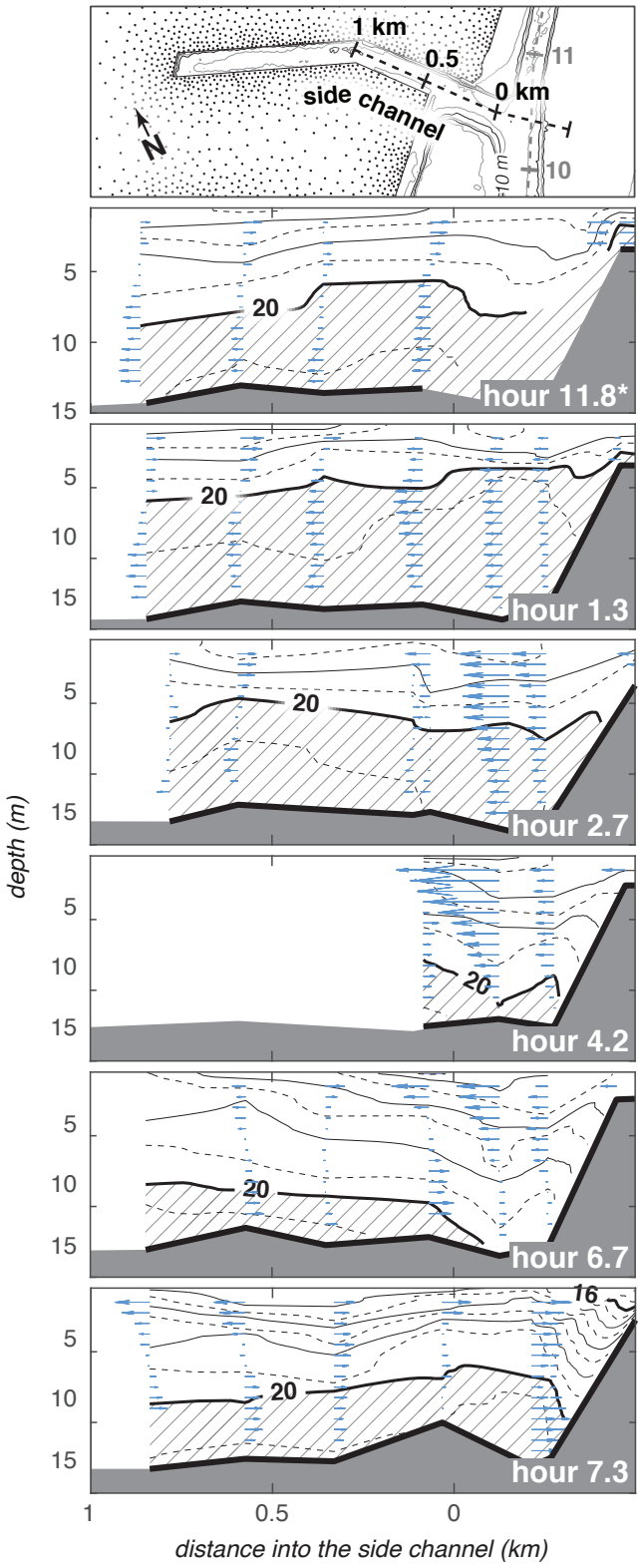

Fig. 7 Across-channel salinity sections in Newark Bay from the end of flood tide (hour 11.8) through early flood (hour 7.3). Arrows indicate across-channel velocities, and shading corresponds to salinities greater than 20 psu. *Conditions at the end of flood tide were observed at the end of the depicted tidal cycle.

baroclinic pressure gradient generates a lateral circulation that exports fresh water from the side channel at the surface. The pressure gradient is reversed as ebb tide progresses (hours 1.3–4.2), as fresh water from the Passaic and Hackensack rivers reduces the surface salinity of the main channel. By maximum ebb (hour 2.7), the reversed pressure gradient strongly draws ebbing fresh water into the side channel, generating a lateral divergence in the main channel (0.25 km; Fig. 7). The response of the main channel to this lateral divergence is the along-channel convergence that forms front S1 (hour 3.0; Fig. 6). Similar interactions between side channels and main channels have been described in laboratory experiments (Langendoen and Karelse 1990), but the resulting along-channel surface front has not been reported. As this front is continuously generated during late ebb tide by the bifurcation of surface outflow, we label this a bifurcation front.

Front S2. The formation and tidal evolution of surface front S2 is shown in roughly ninety-minute intervals in Figure 8 from early ebb to early flood tide. At the start of ebb tide (hour 0.5), the surface salinity gradient increases from Newark Bay toward the Passaic River. Weak surface velocities within Newark Bay are directed landward, and surface velocities within the Passaic are directed seaward. By maximum ebb (hour 2.2), this convergence is advected seaward, and is replaced by surface front S2. Along-channel velocities at the front are divergent. The front, however, remains nearly stationary at the mouth of the Passaic River throughout ebb tide (hours 3.8–6.2). From the consistent location of the front above the Hackensack River outflow, shown in Figure 8 as a mid-depth cross-channel velocity maximum, we hypothesize that the front is generated by the dynamics of the merging Hackensack and Passaic rivers during ebb tide. Because of the geometry of the confluence, Hackensack outflow impinges on outflow from the Passaic. The strong cross-channel shear generated by the impinging flow likely twists the boundary between Passaic and Hackensack outflows into the along-channel direction, generating front S2 (Eq. 1, term 2). This process is consistent with the formation of confluence fronts, which are generated by the along-channel straining of the interface between convergent flows, and are rotated into the along-channel direction by geometry-induced flow asymmetries (De Serres et al. 1999; Riley et al. 2014).

Each of the four fronts described above are generated during ebb tide, propagate landward, and dissipate during flood tide. This process shifts tidal salinity and velocity variability out of quadrature within regions of frontal advection. Propagating lift-off fronts, for example, enhance the near-bed salinity observed at a given location during flood tide, generating a landward tidal-residual salt flux (Geyer and Cannon 1982). We suspect that surface salt fronts that propagate landward during flood tide, on the other hand, generate seaward tidal-residual salt fluxes by weakening the velocities associated with low salinities at a given location during flood tide.

5.3 Quantifying of the influence of fronts on the exchange flow

To quantify the effects of frontal propagation on the exchange flow, we use the Total Exchange Flow (TEF) framework to calculate the exchange flow at four cross-sections: Kill van Kull (mooring KvK), Newark Bay (calculated from measurements at moorings NBc and NBs), the Hackensack River (mooring HR), and the Passaic River (mooring PR). This quasi-Lagrangian framework calculates the both Eulerian and tidal oscillatory components of the exchange flow by tracking volume fluxes in salinity coordinates (Appendix, MacCready 2011; Wang et al. 2015). To use moored observations to estimate the exchange flow, we assume laterally uniform salinity and velocity fields at each cross-section. Time-averaged volume fluxes are constrained to conserve volume, resulting in corrections of less than 5% in Newark Bay and the Hackensack River. The exchange flow within the Passaic requires a correction of 19% to conserve volume; we suspect that this reflects unresolved lateral salinity and velocity heterogeneity, as well as additional freshwater that enters the system downstream of the Little Falls stream gage (USGS gage 01389500). The exchange flow within Kill van Kull is unconstrained due to a lack of measurements in Arthur Kill. However, the estimate of the resulting mean flow through Arthur Kill (70 ± 30 m^3/s) is broadly consistent with

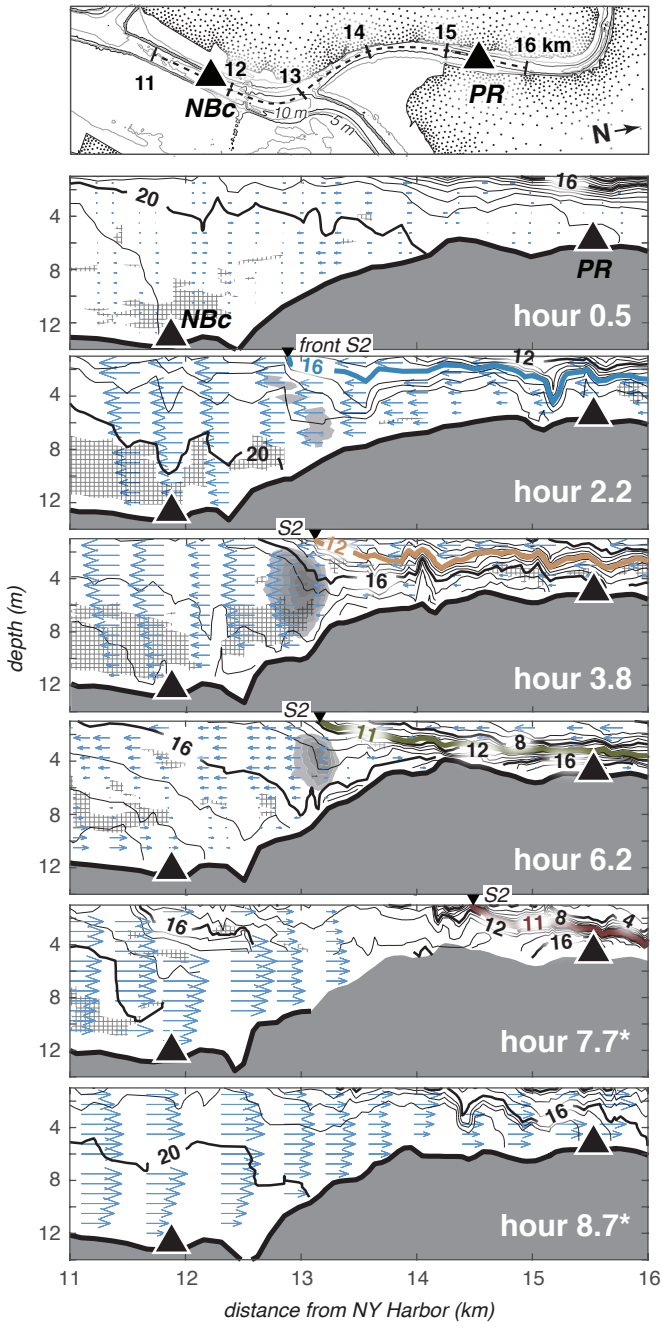

Fig. 8 Along-channel salinity sections at the mouth of the Passaic River from the start of ebb tide (hour 0.5) through maximum flood (hour 8.7). Arrows indicate along-channel velocities, and cross-hatching indicates regions in which the Richardson number is less than 0.5. Contours of westward cross-channel velocities, which emanate from the Hackensack River, are shown in 10 cm/s increments in grey; velocity contours start at 10 cm/s. Salinity isohalines associated with front S2 over time are shown with colored lines.

previous estimates of the through-flow around Staten Island (Kaluarachchi et al. 2003; Sommerfield and Chant 2010). After correcting for volume conservation, the time-averaged net salt fluxes in Newark Bay and in the Hackensack and Passaic rivers are negligible.

The salinity associated with each front observed at a mooring is used to quantify the effect of frontal advection on the tidal oscillatory component of the total salt flux in each region of the sub-estuary. This temporally-varying salinity is the lower limit of the salinity advected landward by a bottom front, or the upper limit of salinity transported landward by a surface front within an individual tidal cycle. This process reveals a distinct maximum of the tidal oscillatory salt flux within salinities associated with frontal advection. This confirms that the advection of saline water

Region	Q_{in}	$Q_{in,\,tidal}/Q_{in,\,total}$	Q_{front}	Q_{front}/Q_{tidal}
Passaic	32	0.58	-9	0.62
Hackensack	140	0.49	—	—
Newark Bay	410	0.51	150	0.61
Kill van Kull	530	0.67	80	0.18

Table 1 Mean exchange flow characteristics within the Newark Bay estuarine network

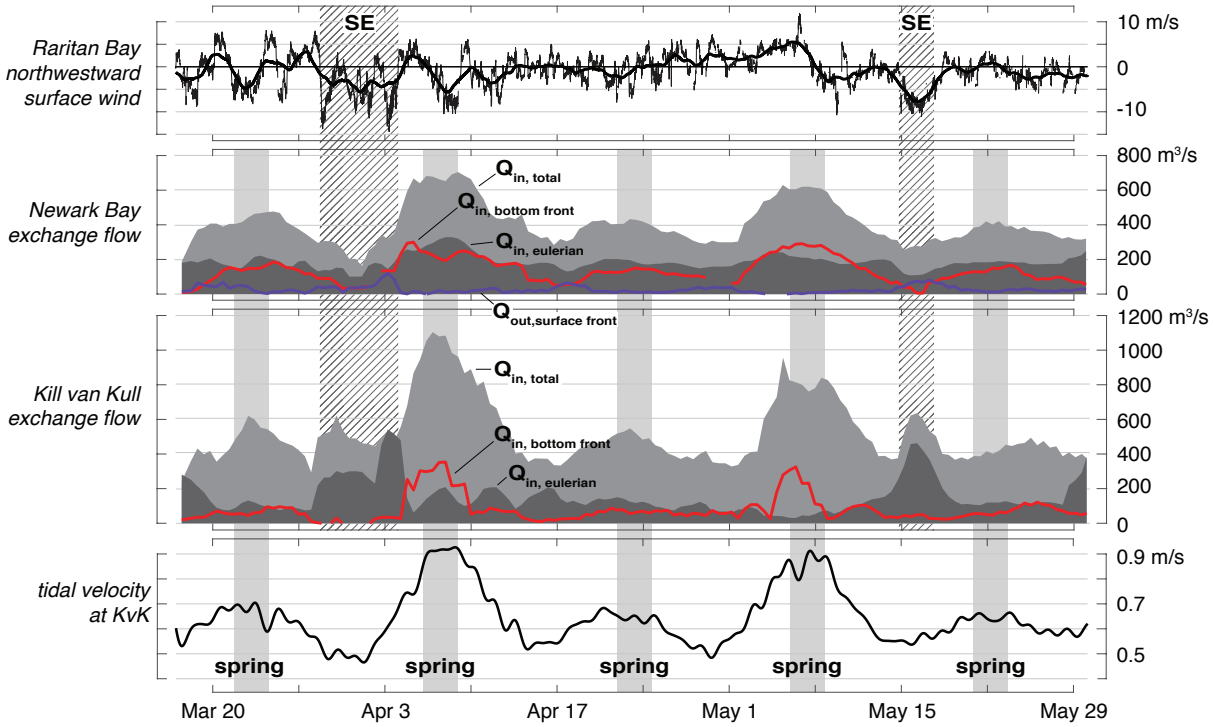

Fig. 9 Time series of environmental conditions and the exchange flow in Kill van Kull and Newark Bay over the period of full moored data coverage in 2016.

behind fronts contributes to the tidal-residual circulation of the estuarine network. However, this contribution substantially varies both over time and between locations.

The characteristics of each region are shown in Table 1, and in Figures 9–10. The exchange flow is strongest in Kill van Kull, and progressively weakens toward the Passaic River. This pattern is the reverse of the mean stratification of the estuarine network, which is strongest in the Passaic and progressively weakens toward Kill van Kull (Fig. 2). The mean ratio of tidal to non-tidal influences on the exchange flow remains at or above 50% throughout the estuarine network, confirming that tidal processes substantially influence the overall structure of the estuary (Table 1, column 2). Of the tidal portion, the advection of fronts S2 and B2 contributes an average of 60% to the exchange flow of the Passaic and Newark Bay, respectively. In Kill van Kull, the proportion of the tidal oscillatory exchange flow associated with frontal advection is much smaller; the tidal propagation of front B1 contributes an average of 18% to the local tidal oscillatory exchange flow. We hypothesize that this may be due to the tidal phase-shift between Kill van Kull and New York Harbor, which limits the landward transport of saline water behind front B1 during flood tide.

Subtidal variability is largest at the mouth of Kill van Kull; fluctuations in the spring/neap cycle explain roughly 60% of observed variations in the strength of the exchange flow. This relationship is driven by fluctuations in the strength of the tidal oscillatory component of the exchange flow. From neap tides to perigean spring tides, the tidal oscillatory exchange flow nearly triples from 300 to 800 m^3/s; this is mirrored in an increase in the magnitude of the component associated

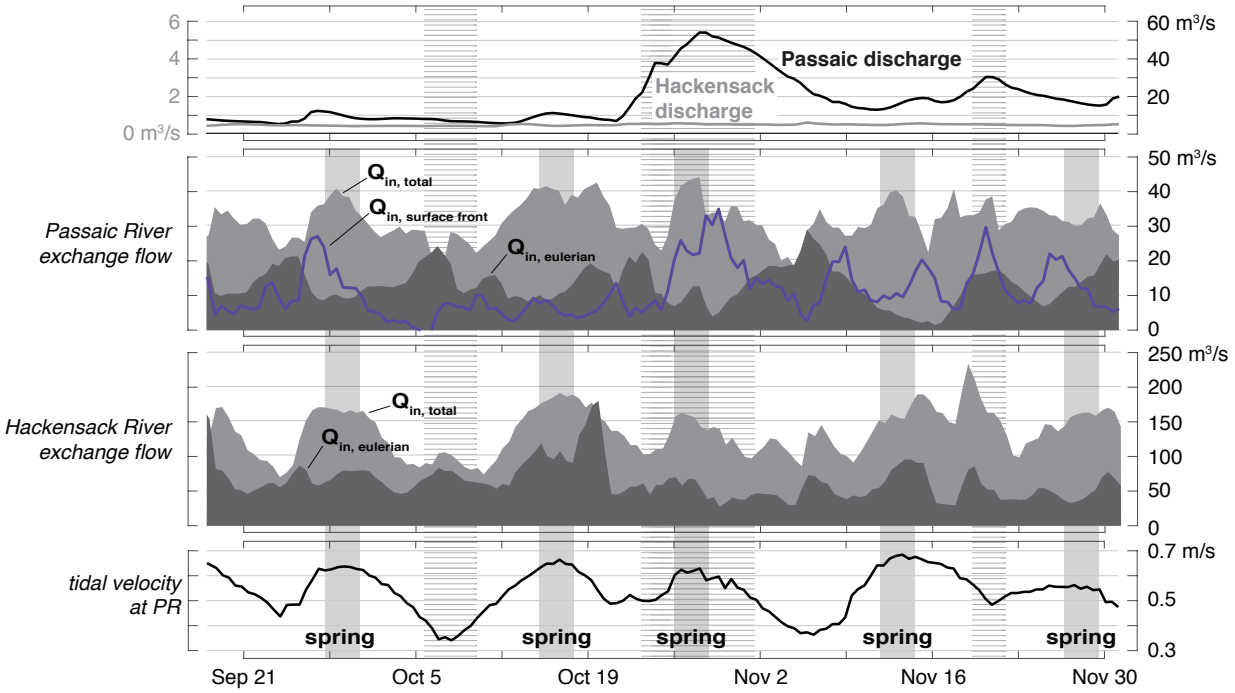

Fig. 10 Time series of environmental conditions and the exchange flow in the Hackensack and Passaic Rivers in 2008 over the period in which fresh water discharge and tidal velocities are statistically-similar to conditions during the 2016 mooring deployment. Periods covered by horizontal lines are excluded from the analysis.

with frontal advection. The Eulerian component of the exchange flow, on the other hand, remains nearly constant aside from brief periods of southeastward winds. Fluctuations in wind stress along 28 degrees west of north explain 60% of the variability of the strength of the Eulerian component of the exchange flow in Kill van Kull; this contribution of wind-driven variability to the exchange flow is similar to a previous estimate of the Kill van Kull—Arthur Kill through-flow (Sommerfield and Chant 2010). Because of the phase-shift between New York Harbor and the Newark Bay estuarine network, the exchange flow within Kill van Kull has two inflow layers — one saline and one fresh. The strong subtidal variability in the exchange flow within Kill van Kull is due to fluctuations in the strength of the saline inflow; the contribution of the fresh inflow layer is largely constant throughout the observation record.

Subtidal exchange flow variability within Newark Bay is driven largely by the spring/neap cycle as well, though the fluctuations are smaller in magnitude than those observed in Kill van Kull. The total exchange flow ranges from 300 m^3/s during neaps to roughly 600 m^3/s during perigean spring tides. This increase in the total exchange flow during spring tides reflects increases in both the tidal oscillatory and Eulerian components of the exchange flow. As fluctuations of each of these components coincide with the spring/neap variations, the relative contributions of each are largely constant throughout the observation record. The volume flux associated with the advection of front B2 similarly increases to 300 m^3/s during perigean spring tides from 100 m^3/s during neaps. The volume flux associated with the landward advection of front S1, on the other hand, increases during neap tides.

The total exchange flow within the Hackensack River is largely influenced by spring/neap variability; however, the individual fluctuations in the spring/neap cycle account for 47% of the variability of the total exchange flow, increasing from roughly 100 to 175 m^3/s from neap to perigean spring tides. Similar to Kill van Kull, the influence of a downstream freshwater source generates an additional layer of inflow associated with a lower salinity than the characteristic outflow of the network. Interestingly, the relative contribution of the saline and fresh inflow to the overall inflow flips over the course of the 2008 observation period. The strength of the saline inflow significantly decreases by 100 m^3/s and the strength of the fresh inflow increases

by the same amount. Despite these trends, the net volume and salt fluxes in the Hackensack are effectively zero throughout the record.

Subtidal fluctuations of the strength of the total exchange flow in the Passaic are weakly influenced by spring/neap variability. Much of this relationship is due to fluctuations in the strength of the tidal oscillatory component of the exchange flow, which ranges from 0–5 m^3/s during neap tides to 30 m^3/s during spring tides. The contribution of frontal advection to the exchange flow, however, is largely influenced by fluctuations in freshwater discharge. The volume flux associated with the landward propagation of front S2 increases by roughly 20 m^3/s during high river flow events, during which the salinity associated with the front decreases by up to 10 psu.

The Newark Bay estuarine network exhibits large spatial variations in stratification, tidal oscillatory fluxes, and strength of the exchange flow. Kill van Kull, for example, contains a three-layer exchange flow that is substantially modified by fluctuations in tidal velocity over the spring/neap cycle. Newark Bay, on the other hand, contains a more typical two-layer exchange flow that is slightly weaker than the exchange flow in Kill van Kull, and more weakly responds to fluctuations in tidal velocity over the fortnightly spring/neap cycle. The exchange flow abruptly weakens landward of the mooring cross-section in Newark Bay. The exchange flow in the Hackensack River is two-thirds weaker than the exchange flow in Newark Bay, and the exchange flow in the Passaic is an order of magnitude smaller than that in Newark Bay. The Hackensack, additionally, contains a three-layer exchange flow. How is the exchange flow modified along the central axis of the estuarine network, and do fronts have a spatial signature over the region of frontal advection? Ongoing analyses seek to address these questions through a combination of field observations and numerical model results.

5.4 The influence of channel geometry on the along-channel structure of the estuarine circulation

The tidal-residual estuarine circulation, or exchange flow, is often portrayed as smoothly-varying along the axis of a partially-mixed estuary (MacCready and Geyer 2010). Recent numerical modeling studies, however, have observed non-uniform gradients in the exchange flow of the Hudson River during spring tides (Wang et al. 2015), suggesting that the exchange flow may be segmented into regions of varying strength. These regions may occur between sites of frontogenesis, as the sign of the tidal oscillatory component of the exchange flow described by Wang et al. (2015) changes from seaward to landward at locations of front generation described by Geyer and Ralston (2015). This contribution of frontal advection to the exchange flow is consistent with the observations of the Newark Bay estuarine network presented in §5.3, and suggests that systems characterized by fronts may also be characterized by an estuarine circulation that is punctuated by mixing regions.

The closest analogue to such systems occurs in fjords, in which mixing between inflowing gravity currents and the fresh surface layer largely determines the salinity of the saline bottom layer within basins (Geyer and Cannon 1982). This tidal residual circulation has been successfully modelled by accounting for both downward and upward entrainment of water (Cokelet and Stewart 1985), which permits a clear examination of the transformation of the salinity of the inflow layer as it travels landward. We hypothesize that frontal estuarine systems may similarly be more clearly modelled through a framework of reflux and efflux, which distinguishes regions in which fresh outflow is entrained into saline inflow from regions in which saline inflow is entrained into fresh outflow. In the coming months, we plan to address this hypothesis by using Cokelet and Stewart (1985)'s framework for estimating reflux and efflux fractions from the hydrographic observations, in addition to using a high-resolution numerical model of the estuarine network to examine the accuracy of this framework on the modelled along-channel structure of the exchange flow.

6 Conclusions

This study has documented the substantial influence of the geometry of an estuary on estuarine dynamics and kinematics by examining Newark Bay, an estuarine network characterized by multiple natural and human-induced channel junctions. Through a combination of shipboard and moored hydrographic observations, we have examined the tidal formation mechanisms of salt fronts as well as the influence of frontal propagation on the tidal-residual exchange flow of the estuarine network. The primary conclusions of this study are as follows:

1. Salt fronts are generated by tidal flow through geometric transitions. Within the study site, these transitions occur at channel junctions. Hydrographic observations confirm that lift-off fronts and tidal intrusion fronts are generated by along-channel convergences through the hydraulic response of stratified flow to channel expansions (Armi and Farmer 1986). In addition, we observe two surface fronts that are not typically described in estuaries. At the confluence of the Passaic and Hackensack rivers, a surface front is generated by the barotropic convergence of tidal flow during ebb tide. This frontogenesis mechanism is well-described at fluvial confluences (De Serres et al. 1999; Riley et al. 2014), but has been infrequently observed within partially-mixed estuaries (Giddings et al. 2012). An additional surface front is generated at the mouth of a side channel during ebb tide in response to an along-channel surface convergence induced by the baroclinic circulation of the side channel. This process of frontogenesis is unique, as seaward channel expansions are typically associated with divergent along-channel velocity fields during ebb tide; we believe that this process has not been documented previously.

2. Junctions also modify front formation and evolution by imposing tidal phase-shifts. Barotropic phase-shifts alternately generate along-channel convergences and divergences in both the salinity and velocity fields, which have the effect of advancing frontogenesis within the period of convergence and weakening fronts within the divergence. These effects are observed on the lift-off front that forms at the mouth of Kill van Kull. Baroclinic phase-shifts at junctions, on the other hand, are found to generate and/or enhance fronts within the main channel through cross-channel convergences and divergences. This is revealed by the formation of a surface front in Newark Bay during a period of lateral divergence induced by the baroclinic circulation of a side channel. This baroclinic circulation concurrently exports salt water at the bed, generating a cross-channel convergence that enhances an along-channel lift-off front.

3. The tidal advection of fronts can substantially contribute to the tidal-residual exchange flow of an estuary. By calculating the exchange flow in salinity coordinates at each cross-section (MacCready 2011), we determine that the landward advection of lift-off fronts is associated with a landward tidal oscillatory salt flux. The landward advection of surface fronts, however, is associated with a seaward tidal oscillatory salt flux by prolonging the local presence of fresh water associated with the previous ebb tide. Within the estuarine network, frontal advection is found to account for up to 50% of the exchange flow. This value varies between regions of the sub-estuary, and changes substantially over the spring/neap cycle.

In the coming months, we plan to examine the influence of the channel geometry on the along-channel structure of the exchange flow through a combination of the hydrographic observations and the results of a high-resolution numerical model of the system. These results, as well as the conclusions for objective (2), will be submitted for peer-reviewed publication, and will also be included within Corlett's doctoral thesis.

Appendix: Exchange flow

At each mooring, the tidally-averaged exchange flow was calculated using the Total Exchange Flow (TEF) framework (MacCready 2011). The framework calculates volume fluxes in salinity coordinates, producing a two-layer exchange flow similar to the structure frequently observed by calculating the exchange flow in depth coordinates (Chant et al. 2018), while also included tidal oscillatory contributions. Within each salinity class, fluxes are calculated as the cumulative sum of fluxes within the more saline salinity classes, as shown in the following equation:

$$Q(s) = \left\langle \int_{A_s} u \, dA \right\rangle \tag{A.1}$$

in which s is the salinity of the class of interest, u is the along-channel velocity, A_s is the cross-sectional area of salinities greater than s, and $Q(s)$ is the sum of tidal-residual volume fluxes within salinity classes greater than s. Consequently, the calculation of the exchange flow requires full water column profiles of both salinity and velocity; observational measurements at the moorings included near-bed and near-surface point measurements of salinity, as well as vertical profiles of horizontal velocity between 0.5 m above the bed and 1 m below the water surface. Velocities between measurements and the bed were extrapolated by assuming a cubic near-bed velocity profile with a no-slip bottom boundary. Velocity measurements were truncated 1 m below the surface for quality control; these surface velocities were filled in by assuming a quadratic surface velocity profile with a free-slip surface boundary to minimize estimation errors. The tidally-varying structure of the vertical salinity profile (fit to the near-surface and near-bed measurements) was calculated from shipboard salinity profiles measured within 500 m of each mooring. Fluxes were averaged over discrete tidal cycles to estimate the effects of episodic tidal processes, such as frontal advection. Tidal cycles were distinguished with local depth-averaged velocities, and stretch from slack water at the start of flood tide to slack water at the end of the following ebb tide.

Fluxes within individual salinity classes ($m^3/s/psu$) were estimated by taking the discrete derivative of the cumulative flux (Q) in salinity space:

$$\frac{\partial Q}{\partial s} = \frac{Q(s + \Delta s) - Q(s - \Delta s)}{\Delta s} \tag{A.2}$$

In this study, $\Delta s = 0.1$ psu. The total landward volume and salt fluxes were calculated as follows:

$$Q(s)_{in} = \int_{s_{in}} -\frac{\partial Q}{\partial s} \, ds \tag{A.3}$$

$$SQ(s)_{in} = \int_{s_{in}} -s\frac{\partial Q}{\partial s} \, ds \tag{A.4}$$

in which the integral is only applied to salinity classes in which tidally-averaged fluxes are directed landward. Similar integrations over seaward salinity classes are used to calculate the total seaward volume and salt fluxes. The negative signs in Equations A.3 and A.4 ensure that the signs of TEF-calculated salinity fluxes are consistent with those calculated in sigma coordinates (i.e. landward fluxes are positive). This correction arises from the inverse relationship between salinity and height above the bed. Following MacCready (2011), representative salinities for both landward and seaward layers were calculated by dividing the layer-specific salt flux by the corresponding volume flux.

The Eulerian component of the exchange flow was calculated by using salinity, velocity, and pressure data within the TEF framework that was tidally-filtered with a low-pass filter with a 33 hour half-amplitude, following Wang et al. (2015) and Lerczak et al. (2006). This permits the effect of tidal processes to be distinguished from subtidal processes in the overall circulation.

References

Alebregtse, N. C., H. E. de Swart, and H. M. Schuttelaars, 2013: Resonance characteristics of tides in branching channels. *Journal of Fluid Mechanics*, **728**, R3.

Allen, F. H. and W. A. Price, 1959: Density currents and siltation in docks and tidal basins. *The Dock and Harbour Authority*, **40(465)**, 72–76.

Armi, L. and D. M. Farmer, 1986: Maximal two-layer exchange through a contraction with barotropic net flow. *Journal of Fluid Mechanics*, **164**, 27–51.

Benjamin, T. B., 1968: Gravity currents and related phenomena. *Journal of Fluid Mechanics*, **31(02)**, 209–248.

Best, J. L., 1987: Flow dynamics at river channel confluences: implications for sediment transport and bed morphology. *Recent Developments in Fluvial Sedimentology*, 27–35.

Blumberg, A. F., L. A. Khan, and J. P. St John, 1999: Three-Dimensional Hydrodynamic Model of New York Harbor Region . *Journal of Hydraulic Engineering*, **125(8)**, 799–816.

Chant, R. J., D. C. Fugate, and E. Garvey, 2011: The Shaping of An Estuarine Superfund Site: Roles of Evolving Dynamics and Geomorphology. *Estuaries and Coasts*, **34(1)**, 90–105.

Chant, R. J., C. K. Sommerfield, and S. A. Talke, 2018: Impact of Channel Deepening on Tidal and Gravitational Circulation in a Highly Engineered Estuarine Basin. *Estuaries and Coasts*, **73(3)**, 587.

Cokelet, E. D. and R. J. Stewart, 1985: The exchange of water in fjords: The efflux/reflux theory of advective reaches separated by mixing zones. *Journal of Geophysical Research: Oceans*, **90(C4)**, 7287–7306.

De Serres, B., A. G. Roy, P. M. Biron, and J. L. Best, 1999: Three-dimensional structure of flow at a confluence of river channels with discordant beds. *Geomorphology*, **26(4)**, 313–335.

Dronkers, J. and J. van de Kreeke, 1986: Experimental determination of salt intrusion mechanisms in the Volkerak estuary. *Netherlands Journal of Sea Research*, **20(1)**, 1–19.

Ebbesmeyer, C. C. and C. A. Barnes, 1980: Control of a fjord basin's dynamics by tidal mixing in embracing sill zones. *Estuarine and Coastal Marine Science*, **11(3)**, 311–330.

Farmer, D. M., E. A. D'Asaro, M. V. Trevorrow, and G. T. Dairiki, 1995: Three-dimensional structure in a tidal convergence front. *Continental Shelf Research*, **15(13)**, 1649–1673.

Geyer, W. R. and G. A. Cannon, 1982: Sill processes related to deep water renewal in a fjord. *Journal of Geophysical Research*.

Geyer, W. R. and D. M. Farmer, 1989: Tide-Induced Variation of the Dynamics of a Salt Wedge Estuary. *Journal of Physical Oceanography*, **19(8)**, 1060–1072.

Geyer, W. R. and D. K. Ralston, 2015: Estuarine Frontogenesis. *Journal of Physical Oceanography*, **45(2)**, 546–561.

Giddings, S. N., D. A. Fong, S. G. Monismith, C. C. Chickadel, K. A. Edwards, W. J. Plant, B. Wang, O. B. Fringer, A. R. Horner-Devine, and A. T. Jessup, 2012: Frontogenesis and Frontal Progression of a Trapping-Generated Estuarine Convergence Front and Its Influence on Mixing and Stratification. *Estuaries and Coasts*, **35(2)**, 665–681.

Hansen, D. V. and M. Rattray Jr., 1965: Gravitational circulation in straits and estuaries. *Journal of Marine Research*, **23(2)**, 104–122.

Hayward, D., C. S. Welch, and L. W. Haas, 1982: York River Destratification: An Estuary-Subestuary Interaction. *Science*, **216(4553)**, 1413–1414.

Kaluarachchi, I. D., M. S. Bruno, Q. Ahsan, A. F. Blumberg, and H. Li, 2003: Estimating the Volume and Salt Fluxes Through Arthur Kill and the Kill van Kull. In *World Water Environmental Resources Congress 2003*, American Society of Civil Engineers, Philadelphia, PA, ISBN 978-0-7844-0683-0, pp. 1–10.

Langendoen, E. J. and M. Karelse, 1990: Laboratory observations of velocity and density fields in the entrance of a harbor on a stratified tidal river. Tech. Rep. 1-90, TU Delft, Department of Hydraulic Engineering, Delft.

Largier, J. L., 1992: Tidal intrusion fronts. *Estuaries*, **15(1)**, 26–39.

—, 1993: Estuarine Fronts: How Important Are They? *Estuaries*, **16(1)**, 1.

Larsen, L. H., 1977: Dispersion of a Passive Contaminant in Oscillatory Fluid Flows. *Journal of Physical Oceanography*, **7(6)**, 928–931.

Lavelle, J. W., E. D. Cokelet, and G. A. Cannon, 1991: A model study of density intrusions into and circulation within a deep, silled estuary: Puget Sound. *Journal of Geophysical Research*, **96(C9)**, 16779.

Lerczak, J. A., W. R. Geyer, and R. J. Chant, 2006: Mechanisms driving the time-dependent salt flux in a partially stratified estuary*. *Journal of Physical Oceanography*, **36(12)**, 2296–2311.

MacCready, P., 2011: Calculating Estuarine Exchange Flow Using Isohaline Coordinates *. *Journal of Physical Oceanography*, **41(6)**, 1116–1124.

MacCready, P. and W. R. Geyer, 2010: Advances in Estuarine Physics. *Annual Review of Marine Science*, **2(1)**, 35–58.

MacDonald, D. G. and W. R. Geyer, 2005: Hydraulic control of a highly stratified estuarine front. *Journal of Physical Oceanography*, **35(3)**, 374–387.

Mathew, R. and J. C. Winterwerp, 2017: Surficial sediment erodibility from time-series measurements of suspended sediment concentrations: development and validation. *Ocean Dynamics*, **67(6)**, 691–712.

Nepf, H. M. and W. R. Geyer, 1996: Intratidal variations in stratification and mixing in the Hudson estuary. *Journal of Geophysical Research: Oceans*, **101(C5)**, 12079–12086.

Pritchard, D. W. and R. E. Bunce, 1959: Physical and Chemical Hydrography of the Magothy River. Tech. Rep. 17, Johns Hopkins University, Baltimore, MD.

Ralston, D. K., W. R. Geyer, and J. A. Lerczak, 2010: Structure, variability, and salt flux in a strongly forced salt wedge estuary. *Journal of Geophysical Research: Oceans*, **115(C6)**, C06005–21.

Rhoads, B. L. and A. N. Sukhodolov, 2001: Field investigation of three-dimensional flow structure at stream confluences: 1. Thermal mixing and time-averaged velocities. *Water Resources Research*, **37(9)**, 2393–2410.

Riley, J. D., B. L. Rhoads, D. R. Parsons, and K. K. Johnson, 2014: Influence of junction angle on three-dimensional flow structure and bed morphology at confluent meander bends during different hydrological conditions. *Earth Surface Processes and Landforms*, **40(2)**, 252–271.

Shrestha, P., S. Su, S. James, P. Shaller, M. Doroudian, C. Firstenberg, and C. Thompson, 2014: Conceptual Site Model for Newark Bay—Hydrodynamics and Sediment Transport. *Journal of Marine Science and Engineering*, **2(1)**, 123–139.

Simpson, J. E. and P. F. Linden, 1989: Frontogenesis in a fluid with horizontal density gradients. *Journal of Fluid Mechanics*, **202**, 1–16.

Simpson, J. H. and R. A. Nunes, 1981: The tidal intrusion front: An estuarine convergence zone. *Estuarine, Coastal and Shelf Science*, **13(3)**, 257–266.

Sommerfield, C. K. and R. J. Chant, 2010: Mechanism of Sediment Trapping and Accumulation in Newark Bay, New Jersey: An Engineered Estuarine Basin. Tech. Rep. 008/07A, Hudson River Foundation, New York, NY.

Suszkowski, D. J., 1978: *Sedimentology of Newark Bay, New Jersey*. Ph.D. thesis, University of Delaware, Newark, DE.

van Maren, D. S., J. C. Winterwerp, M. Sas, and J. Vanlede, 2009: The effect of dock length on harbour siltation. *Continental Shelf Research*, **29(11-12)**, 1410–1425.

Wang, T., W. R. Geyer, P. Engel, W. Jiang, and S. Feng, 2015: Mechanisms of Tidal Oscillatory Salt Transport in a Partially Stratified Estuary. *Journal of Physical Oceanography*, **45(11)**, 2773–2789.

Warner, J. C., D. H. Schoellhamer, J. R. Burau, and S. G. Schladow, 2002: Effects of tidal current phase at the junction of two straits. *Continental Shelf Research*, **22(11-13)**, 1629–1642.

Warner, J. C., D. H. Schoellhamer, and S. G. Schladow, 2003: Tidal truncation and barotropic convergence in a channel network tidally driven from opposing entrances. *Estuarine, Coastal and Shelf Science*, **56(3-4)**, 629–639.